

Deceleration of Madden-Julian Oscillation Speed in NICAM AMIP-type Simulation Associated with Biases in the Walker Circulation Strength

Tamaki Suematsu¹, Hiroaki Miura², Chihiro Kodama³, and Daisuke Takasuka³

¹Atmosphere and Ocean Research Institute, The University of Tokyo

²The University of Tokyo

³Japan Agency for Marine-Earth Science and Technology

November 22, 2022

Abstract

The eastward movement speed of Madden–Julian Oscillation (MJO) events simulated in a 30-year simulation on a global cloud resolving model, nonhydrostatic icosahedral atmospheric model (NICAM), following the atmospheric model intercomparison project (AMIP) protocol, but with a slab ocean, was analyzed and compared with the observation. The simulation reproduced the observed tendency of the MJO to decelerate when they are embedded within stronger Walker circulation, intensified by background sea surface temperature states with larger zonal gradients between the warmer western Pacific and the cooler Indian ocean and eastern Pacific. However, the simulated MJO events displayed a slow bias and occurred disproportionately during El Niño events. These biases were associated with an overestimation of the western Walker circulation cell strength, which was partially counteracted during El Niño events. Our results highlight the importance of accurately reproducing the mean atmospheric circulation for the realistic reproduction of MJO in long term simulations.

1
2 **Deceleration of Madden–Julian Oscillation Speed in NICAM AMIP-type**
3 **Simulation Associated with Biases in the Walker Circulation Strength**

4 **Tamaki Suematsu¹, Hiroaki Miura², Chihiro Kodama³, Daisuke Takasuka³**

5 ¹ Atmosphere and Ocean Research Institute, The University of Tokyo. ² Graduate School of Science, The University
6 of Tokyo. ³ Japan Agency for Marine–Earth Science and Technology

7 Corresponding author: Tamaki Suematsu (suematsu@ori.u-tokyo.ac.jp)

8 **Key Points:**

- 9 • The speed of Madden–Julian Oscillation (MJO) events in a 30-year global simulation
10 with explicit cloud microphysics displayed a slow bias.
- 11 • The tendency of MJO to decelerate with the intensification of the Walker circulation was
12 reproduced in the simulation.
- 13 • The slow bias of simulated MJO was attributed to overly strong western Walker cell,
14 which was partially counteracted by El Niño events.
15

16 **Abstract**

17 The eastward movement speed of Madden–Julian Oscillation (MJO) events simulated in a 30-
18 year simulation on a global cloud resolving model, nonhydrostatic icosahedral atmospheric
19 model (NICAM), following the atmospheric model intercomparison project (AMIP) protocol,
20 but with a slab ocean, was analyzed and compared with the observation. The simulation
21 reproduced the observed tendency of the MJO to decelerate when they are embedded within
22 stronger Walker circulation, intensified by background sea surface temperature states with larger
23 zonal gradients between the warmer western Pacific and the cooler Indian ocean and eastern
24 Pacific. However, the simulated MJO events displayed a slow bias and occurred
25 disproportionately during El Niño events. These biases were associated with an overestimation
26 of the western Walker circulation cell strength, which was partially counteracted during El Niño
27 events. Our results highlight the importance of accurately reproducing the mean atmospheric
28 circulation for the realistic reproduction of MJO in long term simulations.

29

30 **Plain Language Summary**

31 The characteristics of the eastward movement of the Madden-Julian Oscillation (MJO), which is
32 the dominant mode of sub-seasonal variability in the tropical atmosphere, reproduced in a 30-
33 year simulation on an atmospheric model with explicit cloud processes was analyzed. It was
34 found that the simulation was able to reproduce the observed characteristic of the MJO to slow as
35 the large-scale background zonal circulation in the tropics intensifies. However, the simulated
36 MJO displayed a slow bias and occurred too frequently during El Niño events. This was
37 associated with the influence of the El Niño counteracting the biases in the background zonal
38 circulation. The results of the study emphasize the importance of accurately simulating the mean

39 atmospheric states for realistic simulation of the MJO in long-term simulations.

40

41 **1 Introduction**

42 The Madden–Julian Oscillation (MJO) (Madden & Julian, 1971) is the predominant
43 intraseasonal variability in the tropics that is characterized by the slow eastward movement of the
44 convective region, from the equatorial Indian Ocean (IO) to the western Pacific (WP). Far
45 reaching influence of the MJO on the global weather patterns (Roxy et al., 2019; Zhang, 2013)
46 and its potential as a source for predictability in extended-range forecasts (Tseng et al., 2020),
47 makes them a particularly important phenomenon to successfully simulate. However, the
48 realistic simulation of the MJO remains difficult for many state-of-the-art general circulation
49 models (Ahn et al., 2017, 2020; Jiang et al., 2015; H. Kim et al., 2018). This difficulty has been
50 associated with its high sensitivity to model representation of convective processes (Hannah &
51 Maloney, 2011; Holloway et al., 2013), which are large sources of uncertainty in atmospheric
52 simulations (Randall et al., 2003; Stevens & Bony, 2013).

53 The problem of simulating the MJO can be classified into the problem of hindcasting an
54 MJO event as an initial value problem, and to the problem of simulating the MJO as an internal
55 variability of the model reproduced atmosphere. Cloud-resolving models (CRM) with explicit
56 formulations of cloud microphysics, have demonstrated their usefulness for hindcasting MJOs in
57 sub-seasonal simulations (Holloway et al., 2013; Miura et al., 2007; Miyakawa et al., 2014).
58 However, the high computational cost of CRMs hinders the investigation of the latter problem
59 through conducting long-term ($\geq O(10)$ years) simulations.

60 The first ever multi-decadal simulation with explicit cloud microphysics was conducted
61 by Kodama et al. (2015, hereafter K15) on the nonhydrostatic icosahedral atmospheric model
62 (NICAM; Tomita & Satoh, 2004) following an atmospheric model intercomparison project

63 (AMIP) protocol (Gates, 1992), but with a slab ocean model. While the basic statistical
64 properties of the MJO signals in this AMIP-type NICAM simulation (NICAM-AMIP simulation)
65 have been investigated (Kikuchi et al., 2017; K15), the characteristics of the individual MJO
66 events and their relationship with the model reproduced mean states have not been investigated.

67 The eastward movement of the MJO has been indicated to be strongly influenced by the
68 background states of the sea surface temperatures (SST) in both observations (Suematsu &
69 Miura, 2022, hereafter SM22; Wang et al., 2019; Wei & Ren, 2019) and long-term simulations
70 (Chen et al., 2022; Klingaman & Demott, 2020). SM22 revealed that MJO events tend to
71 decelerate when they are embedded within a strong Walker circulation, intensified by
72 background SST states with large zonal SST gradients between the warmer WP and the cooler
73 IO and eastern Pacific (EP). In this study we investigate the reproducibility of this relationship
74 between the MJO speeds and the background states in the NICAM-AMIP simulation.

75

76 **2 Data**

77 **2.1 NICAM-AMIP simulation**

78 We analyzed data from the 30-year integration from NICAM-AMIP simulation from 1
79 June 1978 to 6 January 2009 (K15). The experiment was run with explicit formulation of cloud
80 microphysics (Tomita, 2008), with approximately 14 km horizontal mesh, and 38 vertical layers
81 with the model top at approximately 40 km. The initial atmospheric conditions were obtained
82 from the European Centre for Medium-Range Weather Forecasts Reanalysis-40 (Uppala et al.,
83 2005). The initial land condition was acquired from climatology of a 5-year NICAM simulation
84 at 220 km mesh to reduce the initial shock. A 15 m mixed layer slab ocean model, nudged to
85 SST from the Hadley Centre sea ice and SST dataset version 1 (Rayner et al., 2003), with a

86 relaxation time of 7 days, was coupled with the model. Further details on the experiment have
87 been documented by K15. We examined daily averages of model outputs that were regridded to
88 a resolution of $2.5^\circ \times 2.5^\circ$ to match the observational data for comparability.

89

90 **2.1 Observation and reanalysis**

91 To analyze the observed MJO, we employed interpolated outgoing longwave radiation
92 (OLR; Liebmann & Smith, 1996) data from the National Oceanic and Atmospheric
93 Administration (NOAA), and the daily data of lower level (850 hPa) and upper level (200 hPa)
94 zonal wind (U) velocities from the National Centers for Environmental Prediction-Department of
95 Energy Reanalysis 2 (NCEP-DOE R2; Kanamitsu et al., 2002). Skin temperature from NCEP-
96 DOE R2 was also used to analyze the surface mean states. The SST data were obtained from the
97 NOAA Optimum Interpolated SST version 2 (Reynolds et al., 2002) for the period from 1
98 January 1982 to 31 December 2016. The resolution of SST was reduced to $2.5^\circ \times 2.5^\circ$. We refer
99 to both the observational and reanalysis data as observations for brevity.

100

101 **3 Methodologies**

102 **3.1 MJO detection**

103 The MJO events in both the NICAM-AMIP simulation and observations were identified
104 from time sequences that projected on to the real-time multivariate MJO (RMM) index (Wheeler
105 & Hendon, 2004) from phase 2 to phase 7, while satisfying the following conditions employed
106 by Suematsu and Miura (2018): 1) Phases do not skip forward nor recede backward by more than
107 one phase. 2) The average amplitude is greater than the critical value of 0.8 ($= A_c$). 3) Period of
108 consecutive days with amplitude below A_c is less than 15 days. 4) Transition from phase 2 to

109 phase 7 requires between 20 and 90 days.

110 Calculation of the RMM index followed the procedure of Wheeler and Hendon (2004)
111 except for replacing their procedure to remove the signals of seasonal cycle and longer
112 timescales to the removal of the long-term trend and the application of 20-120 day Lanczos
113 band-pass filter (Duchon, 1979) with 241 symmetric weights. The RMM index sequence of the
114 NICAM-AMIP data was calculated by projecting the simulated data on to eigenvectors of the
115 observational data and by normalizing it using the standard deviations of the projections. MJO
116 events detected by the above method that initiated and terminated between November and April
117 were defined as boreal winter MJO events and were analyzed in this study.

118

119 **3.2 MJO speed estimation**

120 The MJO speeds were estimated following the procedure of SM22. Estimates were made
121 by tracking daily the longitudes at which the 15°S–15°N meridionally averaged OLR anomaly
122 took the minimum value. The tracking was conducted in the restricted longitude ranges of 50°E–
123 120°E for phases 2 and 3, 50°E–150°E for phase 4, 100°E–150°W for phase 5, and 120°E–
124 150°W for phases 6 and 7. The entire longitude ranges (50°E–150°W) were searched on days
125 when the RMM amplitude dropped below A_c . The speed of an MJO event was estimated as a
126 regression coefficient using the dates and longitudes of the tracked minimum OLR anomaly.

127 To confirm the consistency between the MJO speeds estimated from the tracked OLR
128 anomalies in real-space and the trajectory of the MJO events on the RMM phase space, a
129 condition was imposed to ensure that the estimated speeds displayed a linear relationship with
130 the mean angular velocities in the RMM phase space. This was achieved by selecting MJO
131 events that were distributed within 1.5 standard deviation from the regression line between the

132 angular velocities and MJO speeds. The same regression line and standard deviation derived
133 from observations were applied to make selections from the simulated MJO events. Angular
134 velocities were defined as the difference in polar angles between the last day of phase 7 and the
135 first day of phase 2 divided by the number of days between the two. The polar angles were
136 measured from the polar axis in the RMM1 axis in the negative direction.

137

138 **4 Results**

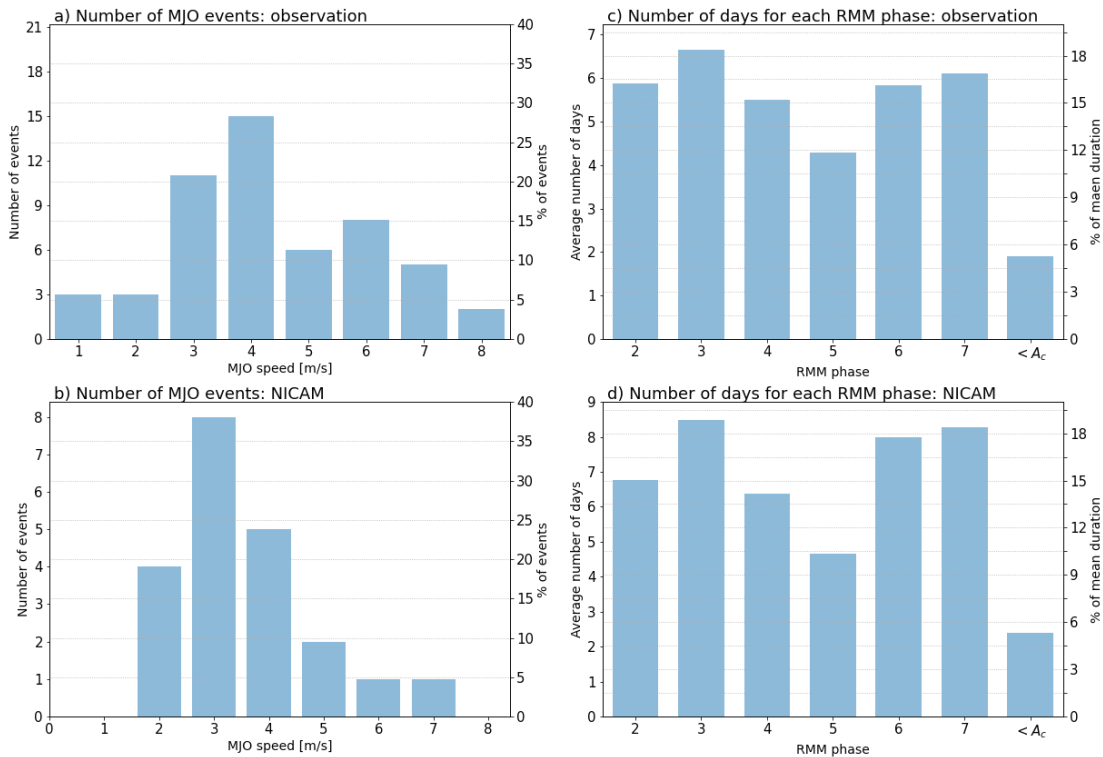
139 **4.1 Basic statistics of detected MJO events**

140 Using the above MJO detection and speed estimation method, 31 MJO events were
141 detected in the NICAM-AMIP simulation between the boreal winters of 1978–1979 and 2007–
142 2008, whereof eastward movement speeds were estimated for 21 events. From observations, 60
143 events were detected between the boreal winters of 1982–1983 and 2015–2016, whereof speeds
144 were estimated for 53 events. The number of MJO events per year in the NICAM-AMIP
145 simulation (1.0 events/year) was underestimated by a factor of 0.56 compared to that observed
146 (1.8 events/year).

147 The frequencies of MJO events in the NICAM-AMIP simulation and observations,
148 categorized by their movement speeds rounded to the nearest integer in m s^{-1} , are shown in
149 Figures 1a and 1b, respectively. The figures indicate that the simulated MJO tended to move
150 slower with smaller variations in their movement speeds compared to observations. The mean
151 speeds were 3.6 m s^{-1} and 4.4 m s^{-1} for the NICAM-AMIP simulation and observations,
152 respectively. These results are consistent with those of Kikuchi et al. (2017).

153 The slow bias of the simulated MJO was consistent with the mean durations of the events,
154 which were 45.0 and 36.2 days for the NICAM-AMIP simulation and observations, respectively.

155 Decompositions of the mean durations by the RMM phases are shown in Figures 1c and 1d.
 156 Days when the RMM amplitude was below A_c were grouped as days with low RMM amplitude.
 157 In all phases, mean durations were longer for the NICAM-AMIP simulation than those for
 158 observations. The mean relative contributions from each RMM phase to the lifetime of MJO
 159 events were remarkably similar. This signified that the deceleration and extended durations of
 160 the MJO events in the NICAM-AMIP simulation resulted from longer persistence of convection
 161 over all phases of the MJO and were not caused by a disproportionate stagnation of convection
 162 nor weakening of the MJO signal over any of the regions from IO to WP.



163
 164 **Figure 1.** (a and b) Number of MJO events binned by their speeds rounded to the nearest integer
 165 in m s^{-1} , (c and d) and average number of days in each RMM phase in an MJO event for
 166 observations (a and c) and NICAM-AMIP simulation (b and d). The ordinates are adjusted so
 167 that the same heights in the histograms represent equal percentages of events in (a) and (b), and

168 mean durations in (c) and (d).

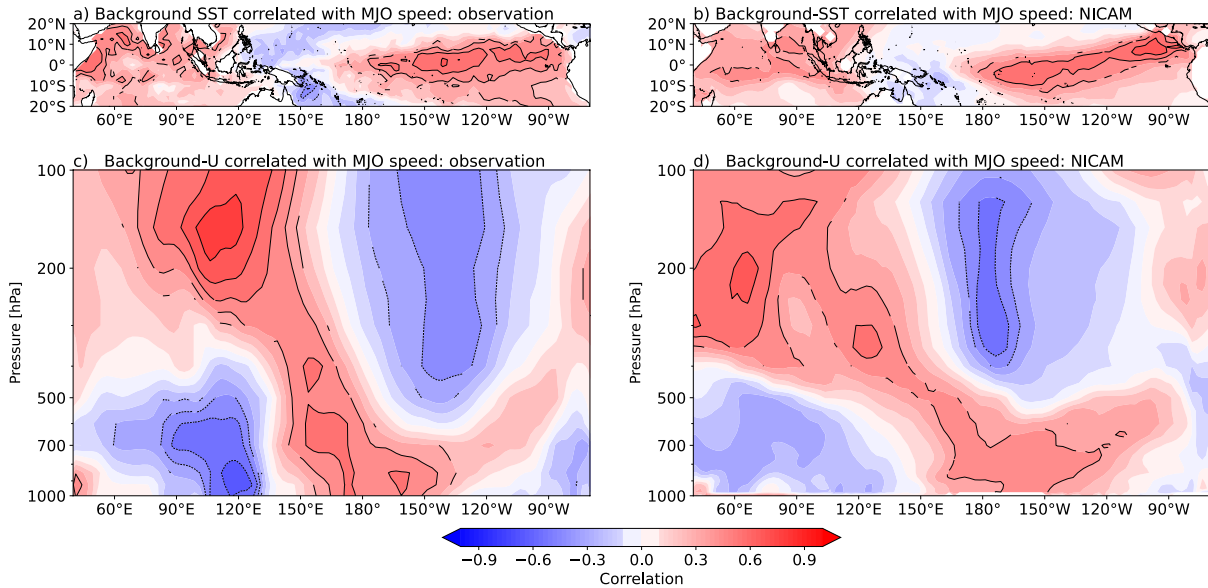
169

170

171 **4.2 Relationship between MJO speeds and background fields**

172 Variations and biases in the simulated MJO speeds were associated with slow changes in
173 the SST fields, which serve as the background SST states for MJO. These were examined and
174 compared with observations. Figures 2a (adapted from SM22) and 2b show the observed and
175 simulated correlation patterns between the background SST on the day of the MJO initiation and
176 the MJO speeds, respectively. Because the longest MJO event in our analysis was 67 days, the
177 background SST was defined as the 90-day low pass filtered SST using a Lanczos filter (Duchon
178 1979) with 241 symmetric weights. Figures 2a and 2b indicate that the NICAM-AMIP
179 simulation reproduced the observed tendency of the MJO to accelerate under El Niño, which
180 reduces the SST gradients between the IO, WP, and EP (Nishimoto & Shiotani, 2013; Pohl &
181 Matthews, 2007; SM2022; Wang et al., 2019; Wei & Ren, 2019). However, the correlation over
182 the WP was weak for the NICAM-AMIP simulation, and it appears that the MJO speeds in the
183 simulation were modulated mainly by the SST variations over the IO and EP.

184 As the thermally direct cells of Walker circulation are modulated by the zonal gradients
185 of the background SST (Bjerknes, 1969), we further examined the relationship between the
186 simulated MJO speeds and the strengths of the Walker circulation that they occurred in. Figures
187 2c (adapted from SM22) and 2d show the correlation pattern of the 5°S–5°N averaged
188 background U with the initiation of the MJO events, for the observations and NICAM-AMIP
189 simulation, respectively. The background circulation was defined using the same filter for
190 defining the background SST.



191

192 **Figure 2.** (a and b) Correlation pattern between MJO speed and background SST, and (c and d)
 193 5°S–5°N averaged U, at the initiation of MJO events for observations (a and c) and NICAM-
 194 AMIP simulation (b and d). The contours indicate the location where the correlations are
 195 significant at a 95% confidence level.

196

197 As shown by SM22, MJO tended to slow under a strong Walker circulation. The general
 198 characteristics of the correlation pattern of the NICAM-AMIP simulation were consistent with
 199 the observations. However, the pattern was distorted as the correlation over the IO was strongest
 200 over the western IO rather than over the Maritime Continent, as in observations.
 201 This indicates that the acceleration of the upper-level (300–200 hPa) easterlies over the western
 202 IO rather than over the Maritime Continent is associated with the deceleration of the MJO speed.
 203 Moreover, the negative correlation of upper-level U over the central Pacific was confined in a
 204 narrow zonal range near the date line for the NICAM-AMIP simulation, while it extended
 205 beyond 120°W in observations. Therefore, while the NICAM-AMIP simulation was able to

206 reproduce the tendency of the MJO to decelerate under a strong western Walker circulation cell,
 207 the distorted correlation pattern of Figure 2d implies that the Walker circulation may be
 208 misrepresented in the NICAM-AMIP simulation. Further discussion on the biases in the
 209 simulated Walker circulation and its possible influence on the simulated MJO is provided in
 210 subsection 4.4.

211

212 **4.3 Enhancement of simulated MJO by ENSO**

213 In the previous subsection, we only inferred the correlations and did not consider any
 214 systematic biases in the simulation with regards to the conditions that may have enhanced or
 215 suppressed the reproducibility of the MJO. Here, we examine the SST conditions that MJO
 216 events in the NICAM-AMIP simulation occurred in, and how they compare with observations.

217 Preceding studies have indicated that zonal SST gradient in which SST increases towards
 218 the WP from both the IO and EP enhances and modulates the eastward movement of the MJO in
 219 observations (Hirata et al., 2013; Suematsu & Miura, 2018, 2022) and simulations (Chen et al.,
 220 2022; H.-M. Kim et al., 2016; Klingaman & Demott, 2020; Miura et al., 2009, 2015). Following
 221 SM22, we examined the occurrences of MJO events by an index of zonal SST gradient defined
 222 as:

223

$$\Delta\text{SST} = \text{SST}_{\text{WP}} - \frac{\text{SST}_{\text{IO}} + \text{SST}_{\text{EP}}}{2} \#(1)$$

224 where SST_{WP} , SST_{IO} , and SST_{EP} are the area-averaged SST over WP (15°S–15°N, 140°E–
 225 160°E), IO (15°S–15°N, 60°E–100°E), and EP (15°S–15°N, 160°W–120°W), respectively.

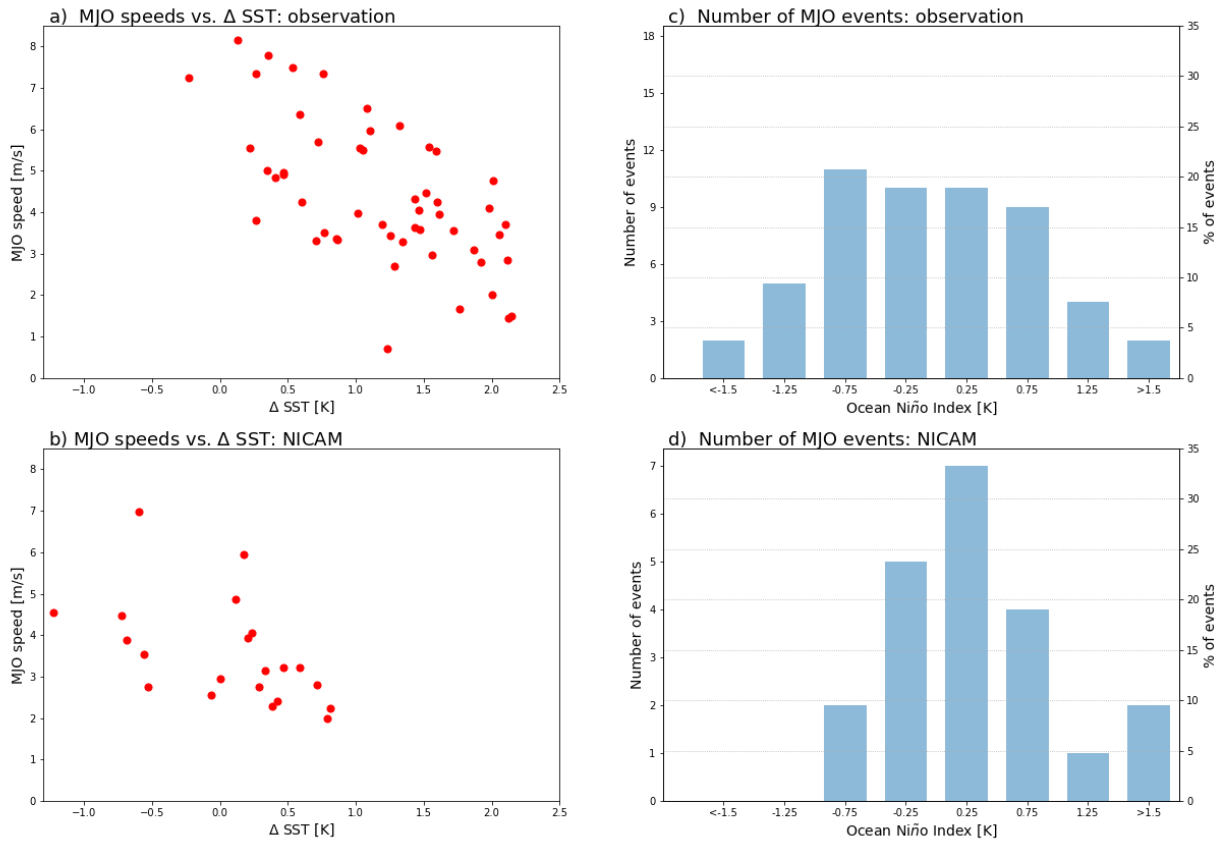
226 The scatter plots displaying the speed of MJO events and ΔSST averaged over 10 days
 227 before initiation are shown in Figures 3a (adapted from SM22) and 3b for observations and the

228 NICAM-AMIP simulation, respectively. MJO events were found to be negatively correlated with
229 Δ SST for both the observations (-0.66) and simulation (-0.51). However, MJO events in the
230 NICAM-AMIP simulation occurred at lower values of Δ SST than those in observations, and a
231 third of the detected events occurred under negative Δ SST conditions.

232 The interannual variability of the SST has been indicated to be the primary cause for
233 changes in Δ SST (SM22). Thus, we examined the frequency of occurrence of MJO events by the
234 strength of the El Niño Southern Oscillation (ENSO), which is the dominant source of
235 interannual SST variability. We employ the Ocean Niño Index (ONI; Trenberth, 1997),
236 calculated as 91 day running means of SST anomalies averaged over the Niño 3.4 region (5°S –
237 5°N , 170°W – 120°W), to evaluate the ENSO phases. Episodes of El Niño and La Niña are
238 defined as periods when the index is > 0.5 K and < -0.5 K, respectively.

239 Figures 3c and 3d show the frequency of MJO events by the ONI, averaged over their
240 lifetimes for observations and the NICAM-AMIP simulation, respectively. MJO events in the
241 observation occurred nearly evenly among the ENSO phases, with slightly more (6%) MJO
242 events during La Niña. However, the reproducibility of the MJO events in the NICAM-AMIP
243 simulation was highly sensitive to the ENSO phase; MJO events occurred more than three times
244 as frequently during El Niño (ONI > 0.5 K, 33%) than during La Niña (ONI < -0.5 K, 10%), and
245 no MJO events occurred under moderate and strong La Niña conditions (ONI < -1.0 K).

246 In the NICAM-AMIP simulation, biases in SST are expected to be small because it was
247 nudged to observation. Thus, we investigate the biases in the mean states of the atmosphere and
248 land surfaces for providing a coherent explanation of the relationship between MJO and SST
249 conditions within the NICAM-AMIP simulation.



250

251 **Figure 3.** (a and b) Scatter plots of MJO speed [m s^{-1}] and Δ SST [K] averaged over 10 days
 252 before the initiation of MJO, and (c and d) histograms of the number of MJO events binned by
 253 the mean values of ONI during their lifetimes at 0.5 K intervals for observations (a and c) and
 254 the NICAM-AMIP simulation (b and d). The ordinates in (c) and (d) are adjusted so that the
 255 same heights in the histograms represent equal percentages of events.

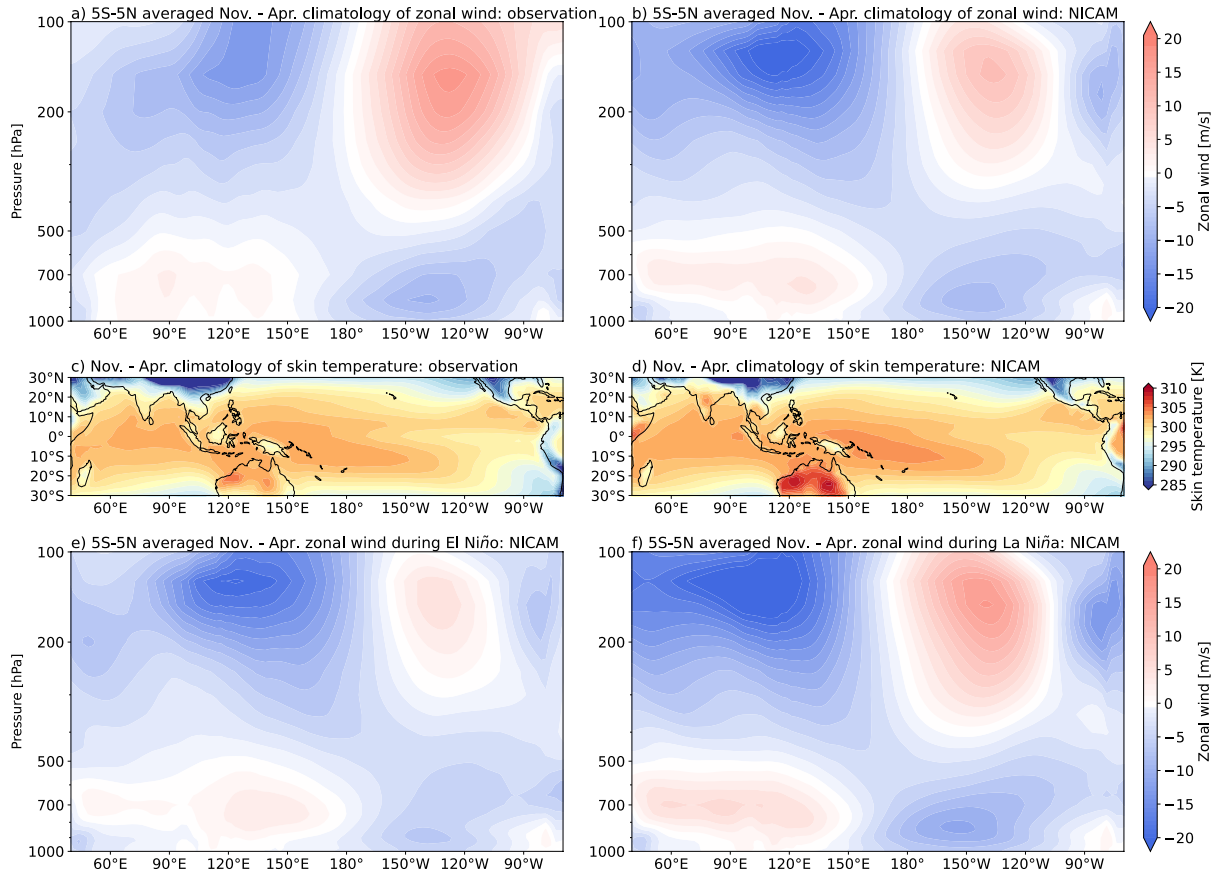
256

257 4.4 Biases in the mean states

258 The mean states of the zonal circulation were compared between observations and the
 259 NICAM-AMIP simulation. Figures 4a and 4b show the November–April climatology of 5°S –
 260 5°N meridionally averaged U for the observations and NICAM-AMIP simulation, respectively.

261 The figures highlight that the NICAM-AMIP simulation reproduced a mean state with an overly
262 strong western Walker circulation cell. The simulated western Walker cell extended beyond
263 60°E, where the western edge of the western cell in the observation was approximately located,
264 and the strength of the upper level (200 hPa–100 hPa) easterlies and low level (700 hPa)
265 westerlies from western IO (approximately 40°E) to the date line, were overestimated. In
266 contrast, the strength of the eastern Walker cell in the NICAM-AMIP simulation was
267 underestimated and was confined to a zonally narrower region between the date line and 120°W,
268 whereas it extended to 90°W for observations.

269 To determine a possible cause for the biases in the strengths of the Walker circulation, the
270 mean states of skin temperature were analyzed (Figures 4c and 4d). Comparisons of the
271 climatological November–April mean skin temperature revealed that there was a large high skin
272 temperature bias over northern Australia in the NICAM-AMIP simulation. Skin temperature was
273 also warmer by 1–2 K in the NICAM-AMIP simulation from IO to WP, which may be due to the
274 bias in longwave cloud radiative forcing shown by K15. The overall pattern of the skin
275 temperature biases was consistent with the intensified Walker circulation over IO to the WP in
276 the NICAM-AMIP simulation.



277

278 **Figure 4.** November to April climatology of (a and b) 5°S – 5°N averaged U [m s^{-1}], and (c and d)
 279 skin temperature [K] for observations (a and c) and NICAM-AMIP simulation (b and d). (e and
 280 f) as in (a and b) but during El Niño (e) and La Niña (f) events in NICAM-AMIP simulation.

281

282 Slow changes in the zonal SST gradient caused by ENSO may counteract or enhance the
 283 biases in the skin temperature and the Walker circulation strength in the NICAM-AMIP
 284 simulation. Figures 4e and 4f compare the November–April mean zonal circulation in the
 285 NICAM-AMIP simulation during El Niño and La Niña, respectively. These figures show that
 286 both sides of the Walker circulation cells were weakened and strengthened during El Niño and
 287 La Niña, respectively. Thus, the overly strong bias of the western Walker cell decreased during
 288 El Niño and increased during La Niña. Additionally, low level (approximately 850 hPa)

289 westerlies from the IO extended to the date line in the NICAM-AMIP simulation during El Niño,
290 which may be associated with the zonal extension of the MJO convective region. MJO events
291 were spuriously enhanced in the NICAM-AMIP simulation during El Niño, when the simulated
292 background circulation of the convectively active region was closer to the observed
293 climatological state. The simulated western Walker cell during El Niño remained stronger than
294 the observed November–April climatology, which may be associated with the slower mean MJO
295 speed in the NICAM-AMIP simulation.

296

297 **5 Summary and Discussion**

298 Simulation of the MJO has long been recognized as a challenging problem. The
299 elimination of convective parameterization in CRM has improved the reproducibility of the MJO
300 as an initial value problem (e.g., Miura et al. 2007; Miyakawa et al. 2014). However, there is
301 limited analysis of MJO events reproduced as internal variabilities of the modelled atmosphere
302 by global CRMs (Kikuchi et al. 2017; K15). In this study, we detected MJO events and analyzed
303 their statistical properties reproduced in a 30-year NICAM-AMIP simulation (K15). The
304 relationship between the variability of MJO speeds, and the background SST and zonal
305 circulation states, identified in a recent study by SM22, was the focus of our analyses.

306 Individual MJO events were identified in the NICAM-AMIP simulation and compared
307 with observations. It was found that the NICAM-AMIP simulation tended to reproduce
308 approximately half the number of MJO events in a given period compared to observations. The
309 simulated MJO events tended to be slower and lasted longer than those observed, indicating that
310 the smaller number of MJO events was partially compensated by longer lifetimes, with regards
311 to the overall activity of the simulated intraseasonal variability.

312 The observed MJO speeds decelerate with the intensification of the Walker circulation
313 cell owing to increased zonal SST gradients between the warmer WP and cooler IO and EP
314 (SM22). The relationship was reproduced well in the NICAM-AMIP simulation; the simulated
315 MJO speed highlighted a clear negative correlation between the Δ SST and the strength of Walker
316 circulation. However, detailed inspection of the SST distributions at which MJO events occurred
317 revealed that simulated MJO occurred during periods when zonal SST gradient was much
318 smaller than for those observed. MJO events were spuriously enhanced and suppressed during El
319 Niño and La Niña events, respectively, in the NICAM-AMIP simulation.

320 Previous studies have also identified model specific enhancements of the MJO by El
321 Niño, associated with moisture fluxes (Chen et al., 2022) and spurious corrections of cold SST
322 biases (Klingaman & Demott, 2020). Biases in the atmospheric mean states were examined for
323 explaining the disproportionate occurrence of MJO events during El Niño. It was revealed that
324 the NICAM-AMIP simulation produced mean states with an overly strong western Walker
325 circulation cell, where the convectively active region of the MJO coincides. El Niño alleviated
326 this model bias towards more realistic background circulation states from the IO to WP, which
327 enabled reproduction of MJO events in the simulation.

328 Questions remain on whether the dynamic processes that modulate the effects of the
329 Walker circulation strength on the MJO speed were realistically reproduced in the NICAM-
330 AMIP simulation. The variability in the composition of convective systems within the MJO
331 envelope should be investigated in a future study to address this uncertainty. For example,
332 whether the observed MJO initiation processes involving interaction between the mixed Rossby-
333 gravity waves and the Walker circulation (Takasuka et al., 2021) was simulated, is of particular
334 interest. It is also of interest to clarify how the inclusion of air–sea interactions in the fully ocean

335 coupled version of NICAM (Miyakawa et al., 2017) could affect the model mean states and the
336 eastward movement of the MJO.

337 **Acknowledgments**

338 T. Suematsu was supported by JSPS KAKENHI Grants 16J07769, 21K13991 and 20H05730. H.
339 Miura was supported by JSPS KAKENHI 16H04048 and 20H05729. C. Kodama and D.
340 Takasuka was supported by JSPS KAKENHI Grants 20H05728. The NICAM–AMIP simulation
341 was performed on the K computer at the RIKEN R-CCS (Proposal numbers hp120279,
342 hp130010, and hp140219).

343 344 **Open Research**

345 NOAA-OLR data are available online (https://psl.noaa.gov/data/gridded/data.interp_OLR.html);
346 The NOAA OI SST V2 high-resolution dataset is available online at
347 (<https://psl.noaa.gov/data/gridded/data.noaa.oisst.v2.highres.html>); NCEP-DOE reanalysis data
348 are available online at (<https://psl.noaa.gov/data/gridded/data.ncep.reanalysis2.html>); and
349 NICAM-AMIP simulation data used in this study are available online at
350 (<https://zenodo.org/record/6348628#.Yi6WgbhUtaR>).

352 353 354 **References**

- 355
356 Ahn, M. S., Kim, D., Kang, D., Lee, J., Sperber, K. R., Gleckler, P. J., Jiang, X., Ham, Y. G., &
357 Kim, H. (2020). MJO Propagation Across the Maritime Continent: Are CMIP6 Models
358 Better Than CMIP5 Models? *Geophysical Research Letters*, 47(11), e2020GL087250.
359 <https://doi.org/10.1029/2020GL087250>
- 360 Ahn, M. S., Kim, D., Sperber, K. R., Kang, I. S., Maloney, E., Waliser, D., & Hendon, H. (2017).
361 MJO simulation in CMIP5 climate models: MJO skill metrics and process-oriented
362 diagnosis. *Climate Dynamics*, 49(11–12), 4023–4045. <https://doi.org/10.1007/S00382-017-3558-4/FIGURES/10>
- 364 Bjerknes, J. (1969). ATMOSPHERIC TELECONNECTIONS FROM THE EQUATORIAL
365 PACIFIC. *Monthly Weather Review*, 97(3), 163–172. <https://doi.org/10.1175/1520->

- 366 0493(1969)097<0163:ATFTEP>2.3.CO;2
- 367 Chen, G., Ling, J., Zhang, Y., Wang, X., & Li, C. (2022). MJO Propagation over the Indian
368 Ocean and Western Pacific in CMIP5 Models: Roles of Background States. *Journal of*
369 *Climate*, 35(3), 955–973. <https://doi.org/10.1175/JCLI-D-21-0255.1>
- 370 Duchon, C. E. (1979). Lanczos Filtering in One and Two Dimensions. *Journal of Applied*
371 *Meteorology*, 18(8), 1016–1022. [https://doi.org/10.1175/1520-0450\(1979\)018<1016:LFIOAT>2.0.CO;2](https://doi.org/10.1175/1520-0450(1979)018<1016:LFIOAT>2.0.CO;2)
- 373 Gates, W. L. (1992). AMIP: The Atmospheric Model Intercomparison Project. *Bulletin of the*
374 *American Meteorological Society*, 73(12), 1962–1970. [https://doi.org/10.1175/1520-0477\(1992\)073<1962:ATAMIP>2.0.CO;2](https://doi.org/10.1175/1520-0477(1992)073<1962:ATAMIP>2.0.CO;2)
- 376 Hannah, W. M., & Maloney, E. D. (2011). The role of moisture-convection feedbacks in
377 simulating the Madden-Julian oscillation. *Journal of Climate*, 24(11), 2754–2770.
378 <https://doi.org/10.1175/2011JCLI3803.1>
- 379 Hirata, F. E., Webster, P. J., & Toma, V. E. (2013). Distinct manifestations of austral summer
380 tropical intraseasonal oscillations. *Geophysical Research Letters*, 40(12), 3337–3341.
381 <https://doi.org/10.1002/grl.50632>
- 382 Holloway, C. E., Woollough, S. J., & Lister, G. M. S. (2013). The Effects of Explicit versus
383 Parameterized Convection on the MJO in a Large-Domain High-Resolution Tropical Case
384 Study. Part I: Characterization of Large-Scale Organization and Propagation. *Journal of the*
385 *Atmospheric Sciences*, 70(5), 1342–1369. <https://doi.org/10.1175/JAS-D-12-0227.1>
- 386 Jiang, X., Waliser, D. E., Xavier, P. K., Petch, J., Klingaman, N. P., Woollough, S. J., Guan, B.,
387 Bellon, G., Crueger, T., DeMott, C., Hannay, C., Lin, H., Hu, W., Kim, D., Lappen, C.-L.,
388 Lu, M.-M., Ma, H.-Y., Miyakawa, T., Ridout, J. A., ... Zhu, H. (2015). Vertical structure
389 and physical processes of the Madden-Julian oscillation: Exploring key model physics in
390 climate simulations. *Journal of Geophysical Research: Atmospheres*, 120(10), 4718–4748.
391 <https://doi.org/10.1002/2014JD022375>
- 392 Kanamitsu, M., Ebisuzaki, W., Woollen, J., Yang, S.-K., Hnilo, J. J., Fiorino, M., Potter, G. L.,
393 Kanamitsu, M., Ebisuzaki, W., Woollen, J., Yang, S.-K., Hnilo, J. J., Fiorino, M., & Potter,
394 G. L. (2002). NCEP–DOE AMIP-II Reanalysis (R-2). *Bulletin of the American*
395 *Meteorological Society*, 83(11), 1631–1644. <https://doi.org/10.1175/BAMS-83-11-1631>
- 396 Kikuchi, K., Kodama, C., Nasuno, T., Nakano, M., Miura, H., Satoh, M., Noda, A. T., &
397 Yamada, Y. (2017). Tropical intraseasonal oscillation simulated in an AMIP-type
398 experiment by NICAM. *Climate Dynamics*, 48(7–8), 2507–2528.
399 <https://doi.org/10.1007/s00382-016-3219-z>
- 400 Kim, H.-M., Kim, D., Vitart, F., Toma, V. E., Kug, J.-S., & Webster, P. J. (2016). MJO
401 Propagation across the Maritime Continent in the ECMWF Ensemble Prediction System.
402 *Journal of Climate*, 29(11), 3973–3988. <https://doi.org/10.1175/JCLI-D-15-0862.1>
- 403 Kim, H., Vitart, F., & Waliser, D. E. (2018). Prediction of the Madden–Julian Oscillation: A
404 Review. *Journal of Climate*, 31(23), 9425–9443. <https://doi.org/10.1175/JCLI-D-18-0210.1>
- 405 Klingaman, N. P., & Demott, C. A. (2020). Mean State Biases and Interannual Variability Affect
406 Perceived Sensitivities of the Madden-Julian Oscillation to Air-Sea Coupling. *Journal of*

- 407 *Advances in Modeling Earth Systems*, 12(2), e2019MS001799.
408 <https://doi.org/10.1029/2019MS001799>
- 409 Kodama, C., Yamada, Y., Noda, A. T., Kikuchi, K., Kajikawa, Y., Nasuno, T., Tomita, T.,
410 Yamaura, T., Takahashi, H. G., Hara, M., Kawatani, Y., Satoh, M., & Sugi, M. (2015). A
411 20-Year Climatology of a NICAM AMIP-Type Simulation. *Journal of the Meteorological*
412 *Society of Japan. Ser. II*, 93(4), 393–424. <https://doi.org/10.2151/jmsj.2015-024>
- 413 Kodama, C., & T., Suematsu, (2022). NICAM AMIP-type simulation data for the article
414 "Deceleration of Madden–Julian Oscillation Speed in NICAM AMIP-type Simulation
415 Associated with Biases in the Walker Circulation Strength". Zenodo.
416 <https://doi.org/10.5281/zenodo.6348628>
- 417 Liebmann, B., & Smith, C. (1996). Description of a complete (interpolated) outgoing longwave
418 radiation dataset. *Bull. Amer. Met. Soc.*, 77, 1275–1277.
- 419 Madden, R. A., & Julian, P. R. (1971). Detection of a 40–50 Day Oscillation in the Zonal Wind
420 in the Tropical Pacific. *Journal of the Atmospheric Sciences*, 28(5), 702–708.
421 [https://doi.org/10.1175/1520-0469\(1971\)028<0702:DOADOI>2.0.CO;2](https://doi.org/10.1175/1520-0469(1971)028<0702:DOADOI>2.0.CO;2)
- 422 Miura, H., Satoh, M., & Katsumata, M. (2009). Spontaneous onset of a Madden-Julian
423 oscillation event in a cloud-system-resolving simulation. *Geophysical Research Letters*,
424 36(13), L13802. <https://doi.org/10.1029/2009GL039056>
- 425 Miura, H., Satoh, M., Nasuno, T., Noda, A. T., & Oouchi, K. (2007). A Madden-Julian
426 Oscillation Event Realistically Simulated by a Global Cloud-Resolving Model. *Science*,
427 318(5857), 1763–1765. <https://doi.org/10.1126/science.1148443>
- 428 Miura, H., Suematsu, T., & Nasuno, T. (2015). An Ensemble Hindcast of the Madden-Julian
429 Oscillation during the CINDY2011/DYNAMO Field Campaign and Influence of Seasonal
430 Variation of Sea Surface Temperature. *Journal of the Meteorological Society of Japan. Ser.*
431 *II*, 93A, 115–137. <https://doi.org/10.2151/jmsj.2015-055>
- 432 Miyakawa, T., Yashiro, H., Suzuki, T., Tatebe, H., & Satoh, M. (2017). A Madden-Julian
433 Oscillation event remotely accelerates ocean upwelling to abruptly terminate the 1997/1998
434 super El Niño. *Geophysical Research Letters*, 44(18), 9489–9495.
435 <https://doi.org/10.1002/2017GL074683>
- 436 Miyakawa, Tomoki, Satoh, M., Miura, H., Tomita, H., Yashiro, H., Noda, A. T., Yamada, Y.,
437 Kodama, C., Kimoto, M., & Yoneyama, K. (2014). Madden–Julian Oscillation prediction
438 skill of a new-generation global model demonstrated using a supercomputer. *Nature*
439 *Communications*, 5. <https://doi.org/10.1038/ncomms4769>
- 440 Nishimoto, E., & Shiotani, M. (2013). Intraseasonal variations in the tropical tropopause
441 temperature revealed by cluster analysis of convective activity. *Journal of Geophysical*
442 *Research: Atmospheres*, 118(9), 3545–3556. <https://doi.org/10.1002/jgrd.50281>
- 443 Pohl, B., & Matthews, A. J. (2007). Observed Changes in the Lifetime and Amplitude of the
444 Madden–Julian Oscillation Associated with Interannual ENSO Sea Surface Temperature
445 Anomalies. *Journal of Climate*, 20(11), 2659–2674. <https://doi.org/10.1175/JCLI4230.1>
- 446 Randall, D., Khairoutdinov, M., Arakawa, A., & Grabowski, W. (2003). Breaking the Cloud
447 Parameterization Deadlock. *Bulletin of the American Meteorological Society*, 84(11), 1547–

- 448 1564. <https://doi.org/10.1175/BAMS-84-11-1547>
- 449 Rayner, N. A., Parker, D. E., Horton, E. B., Folland, C. K., Alexander, L. V., Rowell, D. P., Kent,
450 E. C., & Kaplan, A. (2003). Global analyses of sea surface temperature, sea ice, and night
451 marine air temperature since the late nineteenth century. *Journal of Geophysical Research*,
452 *108*(D14), 4407. <https://doi.org/10.1029/2002JD002670>
- 453 Reynolds, R. W., Rayner, N. A., Smith, T. M., Stokes, D. C., & Wang, W. (2002). An Improved
454 In Situ and Satellite SST Analysis for Climate. *Journal of Climate*, *15*(13), 1609–1625.
455 [https://doi.org/10.1175/1520-0442\(2002\)015<1609:AIISAS>2.0.CO;2](https://doi.org/10.1175/1520-0442(2002)015<1609:AIISAS>2.0.CO;2)
- 456 Roxy, M. K., Dasgupta, P., McPhaden, M. J., Suematsu, T., Zhang, C., & Kim, D. (2019).
457 Twofold expansion of the Indo-Pacific warm pool warps the MJO life cycle. *Nature*,
458 *575*(7784), 647–651. <https://doi.org/10.1038/s41586-019-1764-4>
- 459 Stevens, B., & Bony, S. (2013). What Are Climate Models Missing? *Science*, *340*(6136), 1053–
460 1054. <https://doi.org/10.1126/SCIENCE.1237554>
- 461 Suematsu, T., & Miura, H. (2018). Zonal SST Difference as a Potential Environmental Factor
462 Supporting the Longevity of the Madden–Julian Oscillation. *Journal of Climate*, *31*(18),
463 7549–7564. <https://doi.org/10.1175/JCLI-D-17-0822.1>
- 464 Suematsu, T., & Miura, H. (2022). Changes in the Eastward Movement Speed of the Madden–
465 Julian Oscillation with Fluctuation in the Walker Circulation. *Journal of Climate*, *35*(1),
466 211–225. <https://doi.org/10.1175/JCLI-D-21-0269.1>
- 467 Takasuka, D., Kohyama, T., Miura, H., & Suematsu, T. (2021). MJO Initiation Triggered by
468 Amplification of Upper-Tropospheric Dry Mixed Rossby-Gravity Waves. *Geophysical*
469 *Research Letters*, *48*(20), e2021GL094239. <https://doi.org/10.1029/2021GL094239>
- 470 Tomita, H. (2008). New Microphysical Schemes with Five and Six Categories by Diagnostic
471 Generation of Cloud Ice. *Journal of the Meteorological Society of Japan. Ser. II*, *86A*, 121–
472 142. <https://doi.org/10.2151/JMSJ.86A.121>
- 473 Tomita, H., & Satoh, M. (2004). A new dynamical framework of nonhydrostatic global model
474 using the icosahedral grid. *Fluid Dynamics Research*, *34*(6), 357–400.
475 <https://doi.org/10.1016/j.fluiddyn.2004.03.003>
- 476 Trenberth, K. E. (1997). The Definition of El Niño. *Bulletin of the American Meteorological*
477 *Society*, *78*(12), 2771–2777. [https://doi.org/10.1175/1520-0477\(1997\)078<2771:TDOENO>2.0.CO;2](https://doi.org/10.1175/1520-0477(1997)078<2771:TDOENO>2.0.CO;2)
- 479 Tseng, K. C., Barnes, E. A., & Maloney, E. (2020). The Importance of Past MJO Activity in
480 Determining the Future State of the Midlatitude Circulation. *Journal of Climate*, *33*(6),
481 2131–2147. <https://doi.org/10.1175/JCLI-D-19-0512.1>
- 482 Uppala, S. M., Kållberg, P. W., Simmons, A. J., Andrae, U., da Costa Bechtold, V., Fiorino, M.,
483 Gibson, J. K., Haseler, J., Hernandez, A., Kelly, G. A., Li, X., Onogi, K., Saarinen, S.,
484 Sokka, N., Allan, R. P., Andersson, E., Arpe, K., Balmaseda, M. A., Beljaars, A. C. M., ...
485 Woollen, J. (2005). The ERA-40 re-analysis. *Quarterly Journal of the Royal*
486 *Meteorological Society*, *131*(612), 2961–3012. <https://doi.org/10.1256/QJ.04.176>
- 487 Wang, B., Chen, G., & Liu, F. (2019). Diversity of the Madden-Julian Oscillation. *Science*
488 *Advances*, *5*(7), eaax0220. <https://doi.org/10.1126/sciadv.aax0220>

- 489 Wei, Y., & Ren, H.-L. (2019). Modulation of ENSO on Fast and Slow MJO Modes during
490 Boreal Winter. *Journal of Climate*, 32(21), 7483–7506. [https://doi.org/10.1175/JCLI-D-19-](https://doi.org/10.1175/JCLI-D-19-0013.1)
491 0013.1
- 492 Wheeler, M. C., & Hendon, H. H. (2004). An All-Season Real-Time Multivariate MJO Index:
493 Development of an Index for Monitoring and Prediction. *Monthly Weather Review*, 132(8),
494 1917–1932. [https://doi.org/10.1175/1520-0493\(2004\)132<1917:AARMMI>2.0.CO;2](https://doi.org/10.1175/1520-0493(2004)132<1917:AARMMI>2.0.CO;2)
- 495 Zhang, C. (2013). Madden–Julian Oscillation: Bridging Weather and Climate. *Bulletin of the*
496 *American Meteorological Society*, 94(12), 1849–1870. [https://doi.org/10.1175/BAMS-D-](https://doi.org/10.1175/BAMS-D-12-00026.1)
497 12-00026.1
- 498